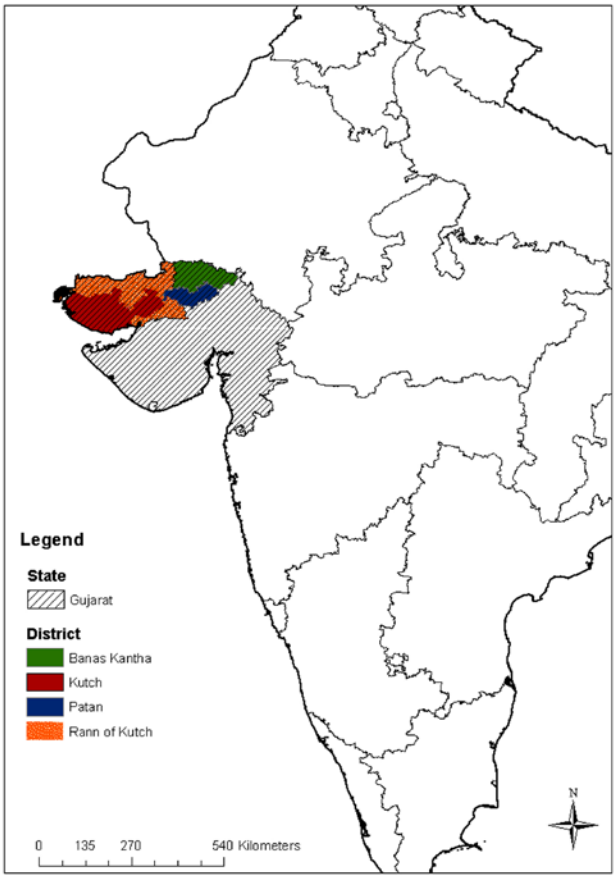

Supporting Figure S1: Study area.

The study is conducted in the state of Gujarat (dashed area) in the districts of Kutch (red), Banas Kantha (green) and Patan (blue). The un-inhabited Rann of Kutch is also shown (in orange).

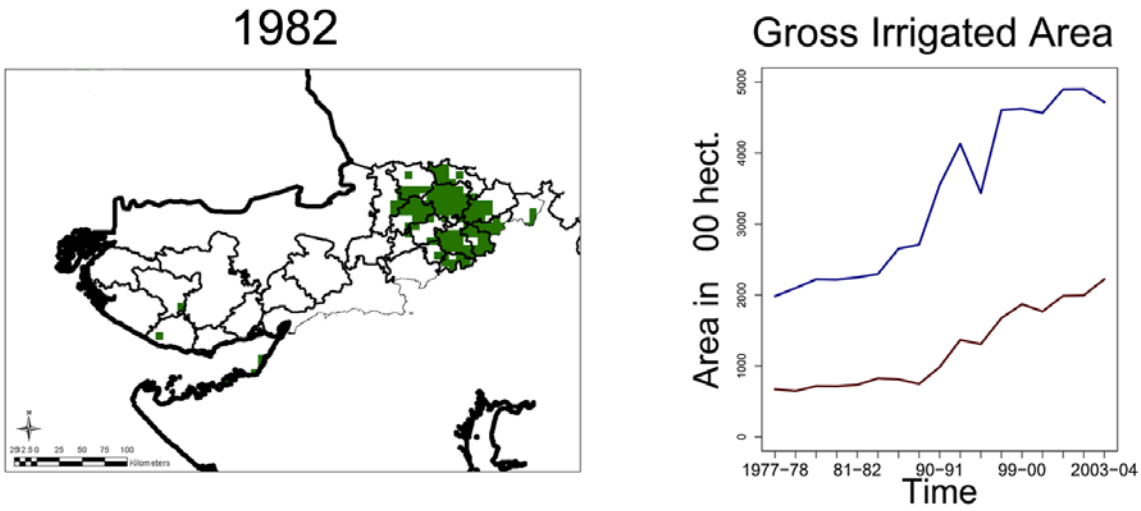

Supporting Figure S2: Historical trends in irrigation in the districts of Kutch and Banas Kantha. To complement our spatial-temporal data, we obtained from the literature historical data on irrigation growth in the region. The map on the left panel shows an NDVI image for January 1982 at an 8 km resolution, obtained from the AVHRR instrument (Tucker et al., 2005). NDVI values > 0.38 are plotted in green, to highlight pixels classified as irrigated (Methods). (Because this threshold value was obtained for MODIS NDVI, we transformed it from MODIS to AVHRR measurements, by fitting a non-linear regression of the form $y \sim a*x^b$, with x=NDVI-MODIS and y= NDVI-AVHRR, and both variables corresponding to the taluka average for the month of January during the years in which MODIS and AVHRR overlapped, 2001-2006). The right panel shows gross irrigated area at the district level for Kutch (red line) and Banas Kantha (blue line) between 1977 and 2004. This additional information on irrigation in the region indicates that the eastern group of talukas, whose spatial extent maps onto the detailed irrigation map of 2009 (Figure 1 and Methods), have been irrigated at least since the beginning of the 1980s.

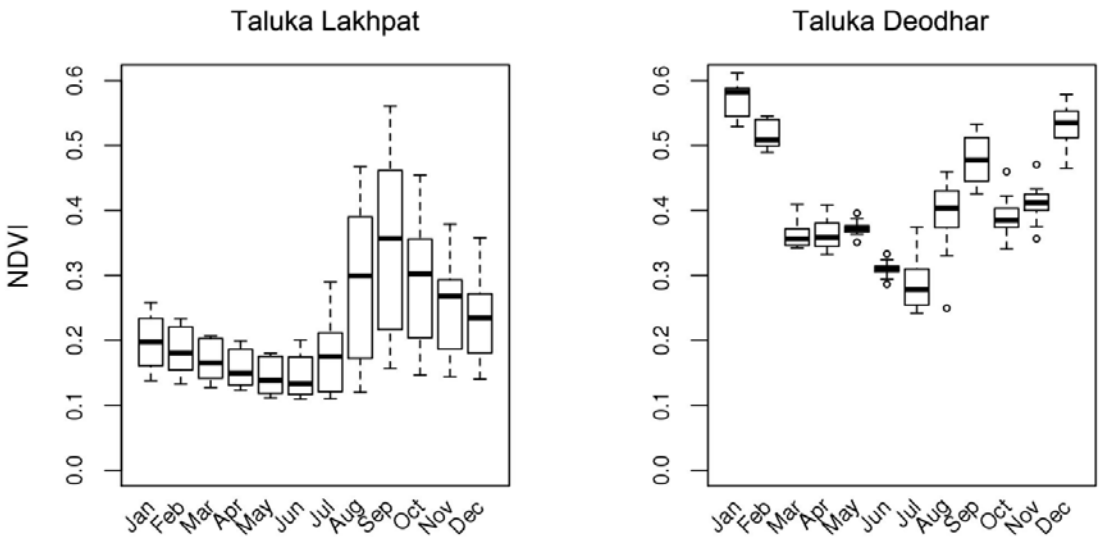

Supporting Figure S3: NDVI seasonality.

The boxplots show the seasonality of average NDVI for the two talukas at the extremes of the irrigation gradient. At the dry end, Lakhpat (taluka #1, Fig. 1 panel A) exhibits only one peak in the vegetation index for the month of September, following the monsoon season. At the other extreme, the highly irrigated taluka of Deodhar (taluka #20, Fig. 1 panel A) displays a bimodal seasonality with a much larger peak in January and much less interannual monthly variation. This January peak is clearly outside the monsoon season and most likely reflects the effect of irrigation on vegetation. Thus, we consider the values of the NDVI vegetation index in that month to formulate a classification of irrigated and non-irrigated land (Methods).

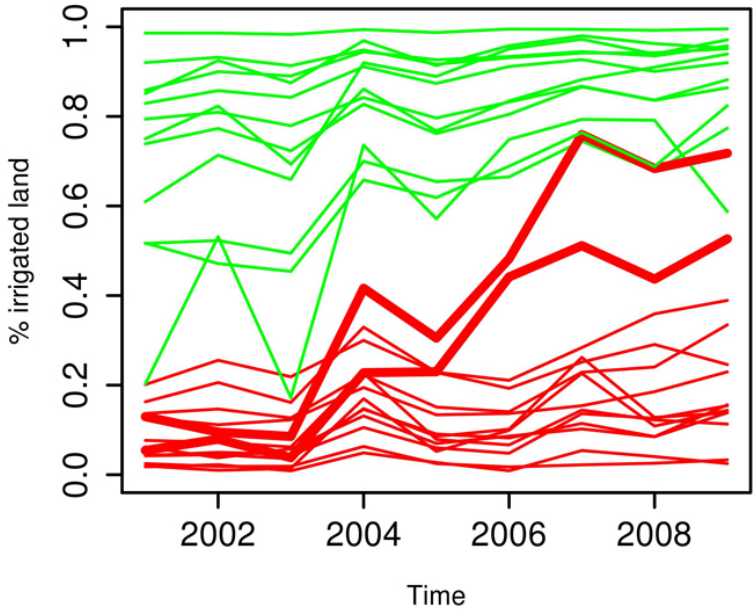

Supporting Figure S4: Temporal changes in estimated irrigation.

Each line represents the annual proportion of the taluka area classified as irrigated between 2001 and 2009, based on the classification procedure using NDVI images (Methods).The green and red lines correspond to talukas in the low and high risk zone according to the results obtained using the grouping algorithm (in Fig. 1 Panel A). The two thicker red lines highlight the talukas where most of the change occurred during the decade; these talukas are located in the southernmost part of the study area (Figure 2 Panel B) and at the boundary of the two regions identified in Figure 1.

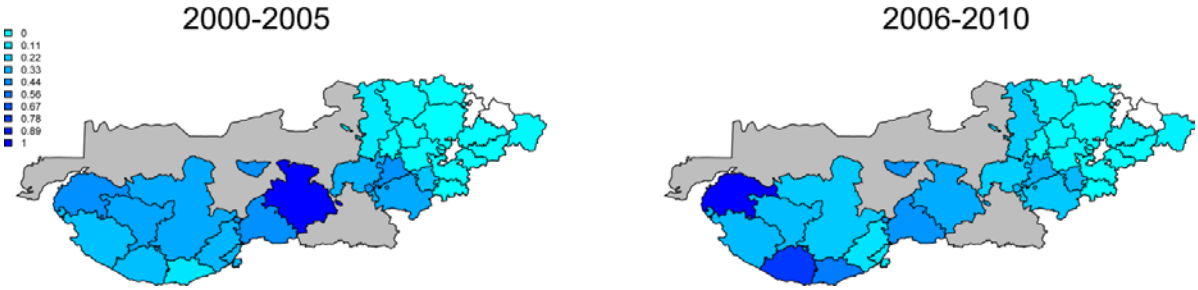

Supporting figure S5: Relative risk of *Plasmodium falciparum* malaria between the years 2000-2010.

Colors from light to dark blue correspond to the level of *P. falciparum* incidence relative to their maximal value. Because the number of cases for this parasite are low (Fig. 1 Panel B), especially in the second half of the decade, the pattern can be quite noisy.

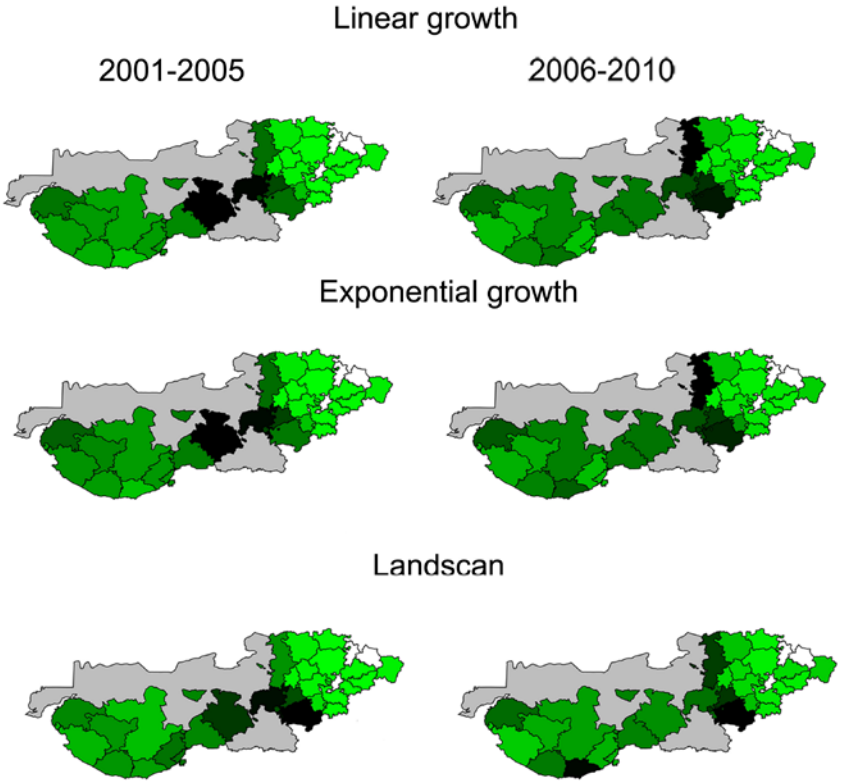

Figure S6: Comparison of results on the spatial distribution of malaria risk for three different ways to estimate population values in between the two censuses of 2001 and 2011.

As a way to corroborate the robustness of our findings to the linear population estimation approach, we also extrapolated the population changes based on exponential growth. To take into consideration possible yearly variation in population we also used the Landscan grid population product from 2001-2011 (Bright, et al., 2002 & Bright, et al., 2012). Because of changes in the methodology from one year to the next, it has been noted that this product should not be used in a time series fashion. Thus,

we relied on Landscan data only for results concerning spatial patterns of prevalence in this figure, and IRS coverage in Fig. S7). See the caption of Figure 3 for further details.
To facilitate comparison, the maps of that figure (obtained with the linear interpolation) are repeated here and included in the top row. The two other methods give similar spatial distributions; in particular, the high risk area remains, at the boundary of the "mature-irrigated" and "low-irrigated" groups of talukas (Figure 1). This is a robust feature with the exception of one additional 'dark' taluka on the coast of Kutch for the Landscan's population estimates (Methods).

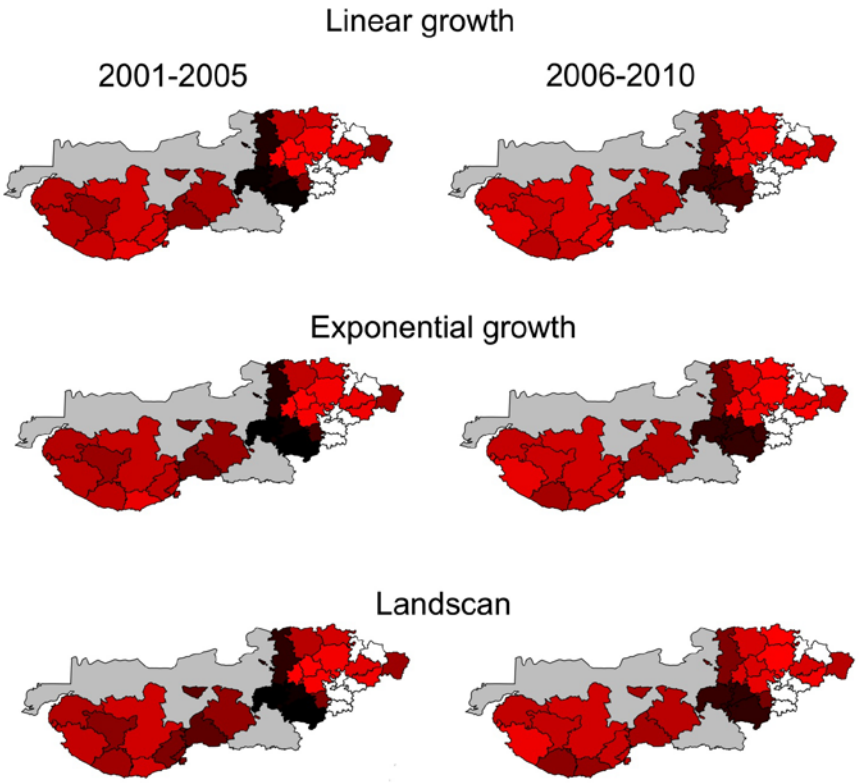

Figure S7: Comparison of results on the spatial distribution of IRS coverage (relative to its maximum value), for three different ways to estimate population values in between the two censuses of 2001 and 2011.
Linear interpolation, exponential interpolation and the gridded product known as Landscan. See the caption of Figures S6 and 3 for more details. Maps of the top row are those of that figure. The high coverage area at the boundary of the eastern and western groups of talukas (Figure 1) is a robust feature.

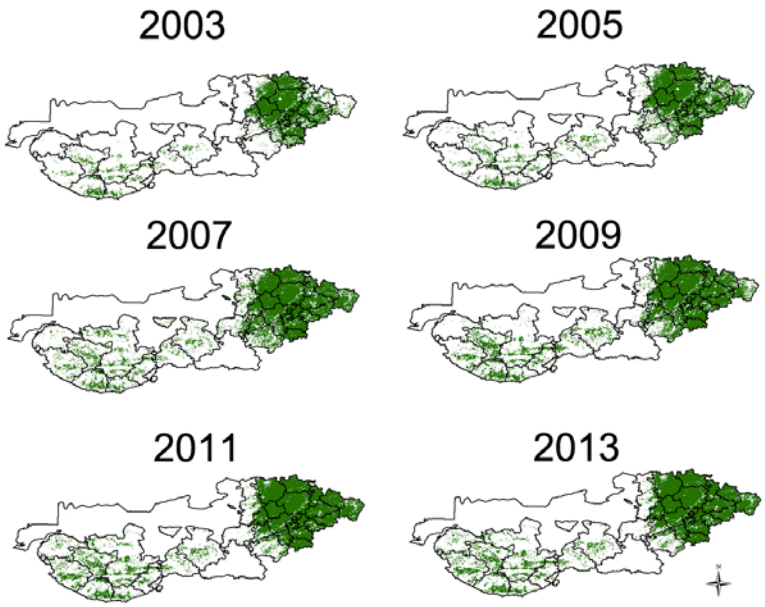

Supporting Figure S8: Reconstruction of irrigation between 2003 and 2013 based on MODIS NDVI images.

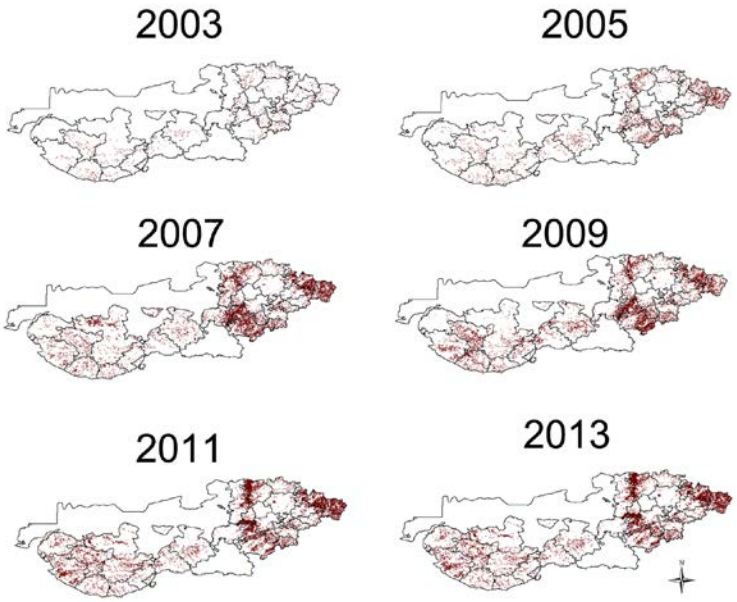

Supporting Figure S9: Spatial change in irrigation between 2001 and subsequent years (2003, 2005, 2007, 2009, 2011, and 2013).

A pronounced change is observed for the talukas at the boundary between the low (or no) irrigation region in the west and the mature irrigated region in the east.

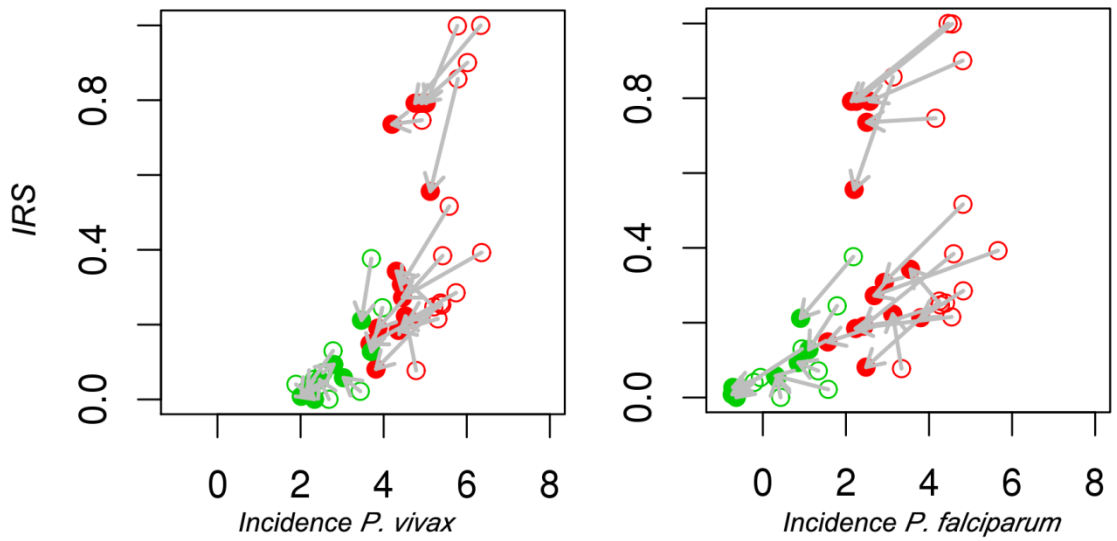

Supporting Figure S10: Trend trajectory of the malaria system and persistence through time of the three identified zones for IRS population coverage and malaria risk, described in the main text.

Each dot in the plot shows the value of control Intervention in terms of percent population covered by IRS as a function of the total incidence per ten thousand people, in logarithmic scale. Empty dots represent the period between 2000 and 2005 and filled dots that between 2006 and 2011. Colors are similar to those in figure 3 Panel C (and 1 A). Despite a downward trend in incidence, the three main regimes depicted in Figure 3 Panel C remain present.